Eur. Phys. J. B **27**, 79–87 (2002)
DOI: 10.1140/epjb/e20020132

THE EUROPEAN PHYSICAL JOURNAL B
EDP Sciences

Optical properties and photonic bands of GaAs photonic crystal waveguides with tilted square lattice

M. Galli[1,a], M. Agio[1], L.C. Andreani[1], L. Atzeni[1], D. Bajoni[1], G. Guizzetti[1], L. Businaro[2], E. Di Fabrizio[2], F. Romanato[2], and A. Passaseo[3]

[1] INFM and Dipartimento di Fisica "A. Volta", Università di Pavia, 27100 Pavia, Italy
[2] NNL-TASC-INFM Nanolithography Beamline, Synchrothron Light Source, 34012 Basovizza-Trieste, Italy
[3] NNL-INFM, Università di Lecce, via per Arnesano, 73100 Lecce, Italy

Received 16 January 2002

Abstract. Reflectance measurements at variable angle of incidence are performed on GaAs photonic crystal waveguides with unconventional square lattices. The technique yields the dispersion of photonic bands for the investigated lattices, as first shown by Astratov *et al.* [Phys. Rev. B **60**, R16225 (1999)]. A sample with a square lattice of air rings and small air fraction yields narrow resonant structures and a dispersion of photonic modes close to that of free photons. Another sample with a square lattice of dielectric squares and large air fraction leads to broader structures and to a dispersion of photonic modes which differs strongly for the two polarizations of light: this sample has a pseudo-gap around 1 micron wavelength. The experimental results are in good agreement with theoretical calculations of the reflectance and of the photonic mode dispersion in the photonic crystal slabs.

PACS. 42.70.Qs Photonic bandgap materials – 81.07.-b Nanoscale materials and structures: fabrication and characterization

1 Introduction

Two-dimensional (2D) photonic crystals embedded in planar waveguides, also known as photonic crystal slabs, are being intensively studied as they can be fabricated at near-infrared or optical wavelengths and yield a good control of light propagation [1–32]. The 2D photonic patterning can produce a band gap in the waveguide plane (xy), while the slab geometry is able to confine the electromagnetic field along the growth direction (z). Defect modes may be introduced in the gap when the 2D structure contains linear waveguides: they form the basis for a new class of photonic devices like bent waveguides, add-drops filters, optical interconnects, etc.

Photonic crystal slabs are subject to the so-called light-line problem: the dispersion of light in the cladding material separates the regions of truly guided modes, which lie below the light line in the first Brillouin zone and have zero radiation losses [6], from quasi-guided modes (or guided resonances) which lie above the light line and have a finite radiative width due to out-of-plane diffraction. Only high index contrast waveguides like the self-standing membrane can support a (small) number of guided modes, while low index contrast waveguides like the GaAs/AlGaAs system have only quasi-guided modes in the whole energy spectrum.

A method to measure the dispersion of quasi-guided modes was first introduced by Astratov *et al.* [8] and consists in measuring the optical reflectivity from the slab surface as a function of incidence angle θ. The reflectance curves display resonant features when the frequency ω and the wavevector parallel to the surface $k_{||} = (\omega/c)\sin\theta$ match those of a photonic mode in the slab: by changing the angle of incidence and the orientation of the sample the dispersion of photonic modes in all directions of the Brillouin zone can be mapped. The measurements of references [8,9,11] were performed on GaAs/AlGaAs waveguides patterned with a triangular lattice of holes, as this structure is the "conventional" one for obtaining a polarization-sensitive photonic gap at relatively small air fractions, or with a one-dimensional lattice of stripes. Similar measurements were performed on GaN/sapphire waveguides, also patterned with a triangular lattice of holes [21].

The study of the photonic bands of different lattices is interesting in order to investigate the dependence of the photonic band dispersion and band gaps on the lattice symmetry and on the dielectric pattern in the unit cell. Various kinds of "nonconventional" lattices and symmetry reduction have been theoretically studied for the 2D case (*i.e.*, without a waveguide) [33–38]. Recently, it was shown [36,37] that a complete 2D photonic gap can be achieved in a square lattice of rotated square rods in a range of filling factors near to the close-packing condition.

[a] e-mail: galli@fisicavolta.unipv.it

In this work we report on the determination of photonic bands by variable-angle reflectance in air/GaAs/AlGaAs waveguides patterned with two unconventional 2D lattices, namely (a) a square lattice of tilted air rings in GaAs dielectric matrix, and (b) a square lattice of tilted squares of GaAs in air. Both samples are fabricated by electron-beam and X-ray lithography followed by reactive-ion etching. The first sample has a small air fraction, leading to narrow and well-defined photonic structures in reflectance; the second sample instead has a large air fraction and broader spectral structures, and it shows a pseudo-gap around 1 micron wavelength. The experimental results are compared with two theoretical treatments: a calculation of the reflectance by the scattering matrix method [10] and a determination of the photonic band dispersion in the photonic crystal slab by an expansion on the basis of waveguide modes for an effective waveguide with the average dielectric constant [39]. Care is taken in treating the polarization properties of the photonic bands: the photonic modes along the symmetry directions of the Brillouin zone are classified as even or odd with respect to a vertical mirror plane coinciding with the plane of incidence, which is the only symmetry plane in a reflectance experiment.

This paper is organized as follows. In Section 2 we describe the sample preparation procedure and the experimental technique. In Section 3 the theoretical methods are illustrated. In Section 4 we present the reflectance results and the photonic band dispersion for the investigated samples, as well as a comparison with the theoretical treatment. Section 5 summarizes the main results.

2 Experimental details

The photonic waveguides investigated in this work were grown in a horizontal LP-MOCVD system (AIXTRON 200 AIX), equipped with a rotating substrate holder, at a growth pressure of 20 mbar. The growth was performed on (100) exactly oriented semi-insulating GaAs substrates at the nominal growth temperature of 750 °C. The structure consists of a 200 nm GaAs buffer layer, followed by 1500 nm of $Al_{0.25}Ga_{0.75}As$ and 500 nm of GaAs as topmost layer. The whole structure was grown at the rate of 4 μm/h and nominally undoped.

Patterning of the waveguides was obtained by X-ray lithography followed by reactive ion etching. The mask was generated by electron beam lithography on a 4×4 mm^2 area and it consists of a chessboard lattice of squares with a period of 500 nm: the lithographed areas on an exposed PMMA film were grown by gold electro-plating deposition before stripping the remaining PMMA. Proximity X-ray lithography performed at LILIT beam line at Elettra Synchrotron (Trieste) was employed to transfer the patterning to the sample. A pre-exposure process step requires the spinning of resists on the sample surfaces: they are chosen of both tones (PMMA 1.07 or SAL 601) in order to have positive and negative transfer of the mask patterning. Also, the shape of the pattern on the sample surface can be controlled by diffraction effects which depend on the gap separation between the mask and the sample. The combined control of diffraction effects and resist development procedure allows to fabricate various kinds of 2D patterns with a wide range of air fractions. Details on the fabrication procedure are given in reference [40].

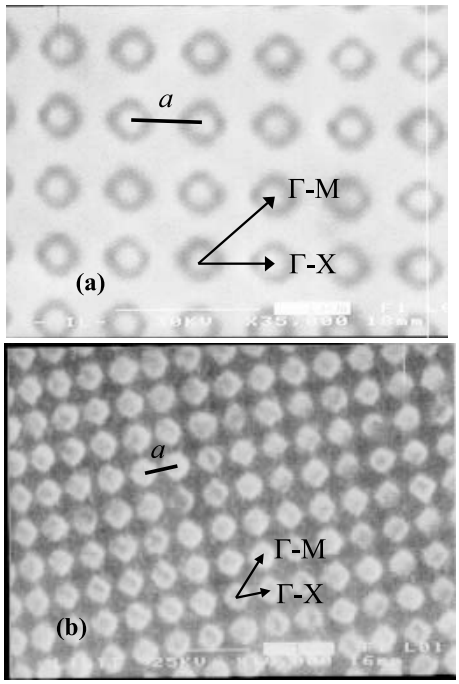

Fig. 1. SEM images of sample L2 (a) and sample RUN3 (b). The lattice constant is $a = 500$ nm for both samples. The main symmetry directions of the square lattice are also indicated.

Finally, a lift-off process was performed by evaporating 10 nm of nickel and then stripping the residual resist. Nickel in fact showed an extremely high selectivity to the reactive ion etching (RIE) performed by an Induced Coupled Plasma RIE reactor in a atmosphere of 95% SiCl4 and 5% of Ar and biasing the cathode at 230 eV. Etching time was 5 min, leading to an etch depth of about 1 μm in the patterned regions.

In Figure 1 we show scanning-electron micrographs of the two samples studied in this work. For both samples, the lattice constant of the square Bravais lattice along the [100] direction is $a = 500$ nm. The first sample (called L2, Fig. 1a) has been patterned on PMMA resist resulting in a 2D pattern lattice consisting of air rings with an air fraction of 12%: the shape of the rings reflects the tilted squares of the mask, where the squares are rotated by 45° with respect to the axes of the Bravais lattice. The 2D pattern of the second sample (named RUN3, Fig. 1b) obtained by exposing a SAL601 resist film consists of squares of dielectric, which are also tilted by 45°: the dielectric fraction is close to 28%. A schematic picture of the two unit cells and of the 2D Brillouin zone is shown in Figure 2.

The variable angle specular reflectance was measured in the 0.5–1.5 eV spectral range by means of a Fourier

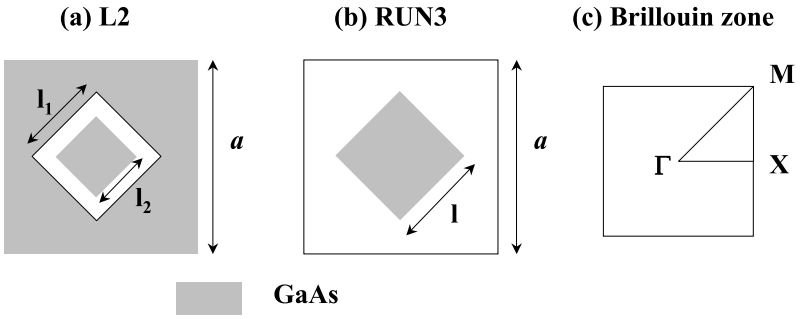

Fig. 2. Unit cell of the two samples (a,b) and 2D Brillouin zone (c). The parameters assumed in the calculations are: (a) sample L2: $l_1 = 0.47a$, $l_2 = 0.32a$, leading to an air fraction $f_{air} = 0.12$; (b) sample RUN3: $l = 0.53a$, leading to a dielectric fraction $f_{diel} = 0.28$. The lattice constant is $a = 500$ nm.

transform spectrometer (Bruker IFS-66) at a spectral resolution of 1 meV. The samples were illuminated by the light beam from a broadband tungsten- halogen lamp that was collimated and focused onto the sample surface with a spread angle of $\pm 1°$. The angle of incidence θ was varied from 5° to 60° with steps of 2.5°, and the plane of incidence was chosen to be perpendicular to the sample surface. A liquid-nitrogen-cooled InSb photodiode was used as a detector and a silver mirror was used as absolute reflectance reference. Measurements were performed for light incident along the high symmetry orientations Γ-M and Γ-X of the 2D samples, both for transverse electric (TE) and Transverse magnetic (TM) polarized light by means of a calcite Glann-Taylor polarizer. Spectroscopic ellipsometry measurements in the range 0.9–4 eV were used in a complementary way to characterize the quality and the thickness of the waveguides before patterning.

3 Theory

Two theoretical approaches are developed in order to interpret the reflectance experiments. In the first one [39], the photonic bands of the patterned waveguide at the in plane Bloch vector $\mathbf{k}$ are calculated by expanding the magnetic field as

$$\mathbf{H}_k(\mathbf{r}) = \sum_{\mathbf{G}\alpha} c_{\mathbf{k}+\mathbf{G},\alpha}\, \mathrm{e}^{\mathrm{i}(k+G).r}\, \mathbf{h}_{\mathbf{k}+\mathbf{G},\alpha}(z) \qquad (1)$$

where $\mathbf{h}_{\mathbf{k}+\mathbf{G}\alpha}(z), \alpha = 1, 2, ...$ are the guided modes of the air/GaAs/AlGaAs waveguide at wavevector $\mathbf{k}+\mathbf{G}$ and the patterned layers (core and lower cladding) are taken to have an average dielectric constant. The second-order equation for the magnetic field becomes a linear eigenvalue problem for the expansion coefficients $c_{\mathbf{k}+\mathbf{G},\alpha}$ with the waveguide modes being coupled by the off-diagonal components of the inverse dielectric tensor. Just like in the case without waveguide, a finite cutoff must be imposed for the reciprocal lattice vectors $\mathbf{G}$ and Ho's method of inverting the dielectric matrix has to be used for faster convergence [41]. This approach yields the energy dispersion of the guided modes whose energies lie below the light lines of the upper and lower claddings, as well as of the modes which lie above the two light lines when folded in the first Brillouin zone. It neglects coupling of the latter states to the leaky modes of the waveguide, therefore it does not yield the imaginary part of the energy that corresponds to intrinsic radiation losses (out-of-plane diffraction in a transmission experiment). The resonance energies of quasi-guided modes are of central interest for the interpretation of the present experiments, since they correspond to the spectral positions of the resonant structures in reflectance, which arise when a quasi-guided mode is excited by the incoming beam.

In the second approach [10] we calculate the reflectance and transmittance (and also the diffraction) of the layered system by a plane wave expansion in each layer, which yields the complex photonic bands at given in-plane wavevector $\mathbf{k}$ and frequency ω, and by propagating the field along the multilayer *via* a scattering matrix. In the present case we have five layers: air, patterned GaAs, patterned and unpatterned AlGaAs, GaAs substrate. The frequency-dependent complex dielectric constants of GaAs and AlGaAs are used in the calculation [42]. This numerical method is an exact solution of Maxwell equations and it contains all radiative effects in the structure.

The symmetry properties and selection rules are now discussed, generalizing previous work on 2D photonic crystals [43,44]. For a wavevector $\mathbf{k}$ along a symmetry direction of the lattice (in the 2D case, the Γ-X and Γ-M directions), specular reflection with respect to a vertical plane ($\mathbf{k}$,$\mathbf{z}$) is a symmetry operation and the TE or TM polarization of the incident wave is maintained in reflectance. Correspondingly, the photonic bands can be classified as even or odd with respect to vertical mirror symmetry. They are probed by a polarized incident wave as follows: a TM-polarized wave couples to even bands, a TE-polarized wave couples to odd bands. Note that for the present asymmetric air/GaAs/AlGaAs structure there is no mirror symmetry with respect to the waveguide plane (unlike in the homogeneous 2D case [45]).

The parameters of the 2D structures assumed for the calculations are indicated in Figure 2. The thicknesses of the core and cladding layers are taken from ellipsometry results and are given in the inset to Figure 3 (see discussion below). For the calculation of the photonic bands in the waveguide we use only the thickness of the core layer, since the patterned lower cladding is assumed to

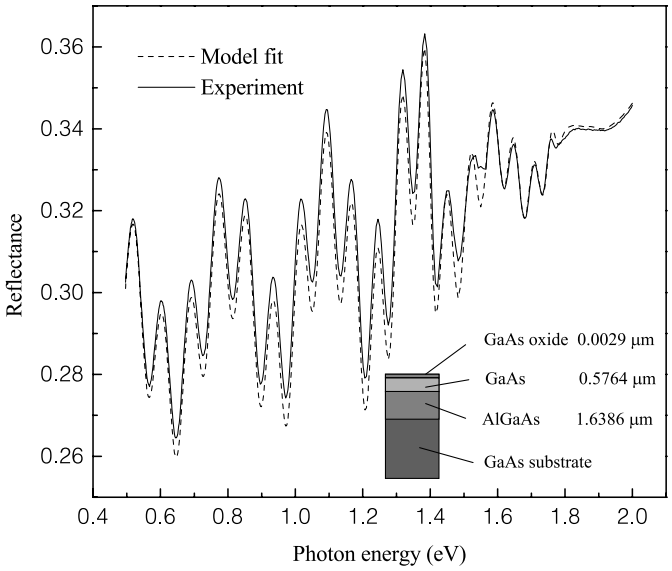

Fig. 3. Experimental (solid) and calculated (dashed) normal incidence reflectance of the GaAs waveguide slab. Inset reports the layer thicknesses as obtained from the best-fit procedure.

be of semi-infinite extent. For the reflectance calculation instead we need also the etch depth: this is taken to be 1 μm for sample L2 and 0.95 μm for sample RUN3, respectively. These values are close to those estimated from etching rates and were slightly adjusted in order to reproduce the interference fringes in the reflectance spectra.

4 Results and discussion

The GaAs/AlGaAs planar waveguide was optically characterized before patterning in order to determine the thickness of the different layers to be used in the calculation of photonic bands and reflectance spectra of the patterned structure. Ellipsometric spectra from 1.4 to 5 eV and near-normal reflectance in the 0.4 to 6 eV range were measured and simultaneously fitted to a 4-layer model which includes the waveguide structure with a thin native oxide layer on top. Figure 3 shows the normal-incidence reflectance of the overall waveguide structure together with the best-fit curve in the 0.5–2 eV energy range. We note that reflectance spectrum is characterized by strong oscillations that result from the combination of two different interference patterns: a slowly-varying long-period one and a fast-varying short-period one. These are related to the core layer and the core + cladding layers of the AlGaAs/GaAs waveguide respectively. The overall interference pattern is well reproduced by the four-layer model and the thickness of each layer as obtained from the best-fit are reported in the inset of Figure 3.

The variable angle reflectance spectra of the L2 sample are presented in Figures 4a and 5a for TE and TM polarized light incident along the Γ-M direction of the 2D Brillouin zone. The corresponding calculated spectra are shown in Figures 4b and 5b. Similar results are obtained for light incident along the Γ-X orientation (not shown here). The angle of incidence θ ranges from 5° to 60° in steps of 5° (measurements were performed at angular intervals of 2.5° but only half of them are shown) and each curve corresponding to a different θ value was vertically shifted by a constant quantity in order to better appreciate the angular evolution of reflectance.

As for the unpatterned waveguide, what can first be noticed in reflectance spectra are pronounced interference oscillations arising from the multilayer structure of the system. The double interference pattern is still observed even though in this case the period of the oscillations changes slightly upon increasing the energy. This effect could be explained by considering that for increasing frequencies the electromagnetic field is mainly confined within the dielectric regions of the patterned waveguide rather than the air regions [45]. This, in turn, leads to an effective refractive index 'seen' by the incident radiation that increases with increasing frequencies, therefore giving rise to a frequency dependent period of the interference. The interference pattern is well reproduced by the calculation with the etch depth of 1 μm. Superimposed on this complex interference background, several narrow structures (indicated by vertical bars in Figures 4a and 5a for $\theta = 5°$ and $\theta = 60°$) are clearly observed. By increasing the angle of incidence θ, the energy positions of these sharp features display a well-defined dispersion towards either lower or higher energies.

As previously reported for GaAs/AlGaAs [8,9,11,15], GaN/sapphire [21] and Silicon-on-Insulator systems [46] we ascribe these narrow structures to resonant coupling of the incident external radiation to quasi-guided modes of the patterned waveguide, occurring whenever phase-matching conditions are fulfilled. When both energy and in-plane wavevector $\mathbf{k}_{||} = (\omega/c)\sin\theta$ match those of a propagating mode, coupling to the waveguide occurs and a corresponding resonance appear in reflectance. Upon varying the angle of incidence, the in-plane wavevector changes accordingly, and the different matching conditions lead to smooth energy dispersion of the resonances.

This interpretation is strongly supported by the comparison of the experimental spectra with the calculated ones. There is an overall good agreement: both the multiple interference pattern and the observed resonances are well accounted for by calculations. We notice that intensity and shape of the structures changes markedly with angle, showing a variety of maxima, minima and dispersive-like lineshapes. However, they remain relatively narrow and well defined even for high θ values, exhibiting a FWHM of the order of 10^{-2} eV. While the amplitude of the resonances is related to the coupling strength to guided modes, their width is mainly determined by radiative and dissipative losses, which are expected to be low for patterned waveguides with a low air fraction [12,23]. In fact, despite some surface inhomogeneity possibly coming from the etching process, the observation of relatively narrow features in the L2 sample can be considered as an indication of good guiding properties. This suggests that samples with low air fraction may be useful for achieving low- loss propagation, although the relatively weak

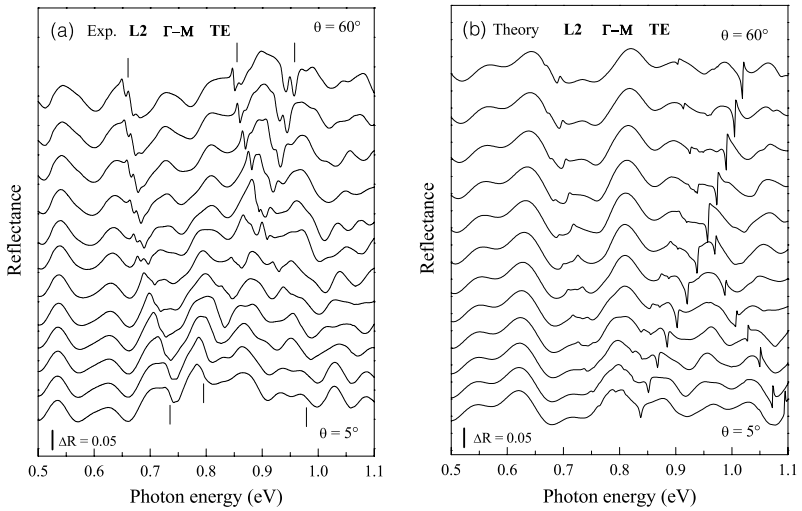

Fig. 4. Sample L2: experimental (a) and calculated (b) variable angle reflectance for TE polarized light incident along the Γ-M direction. The angle of incidence is varied in steps of 5°. The different curves are shifted vertically for clarity.

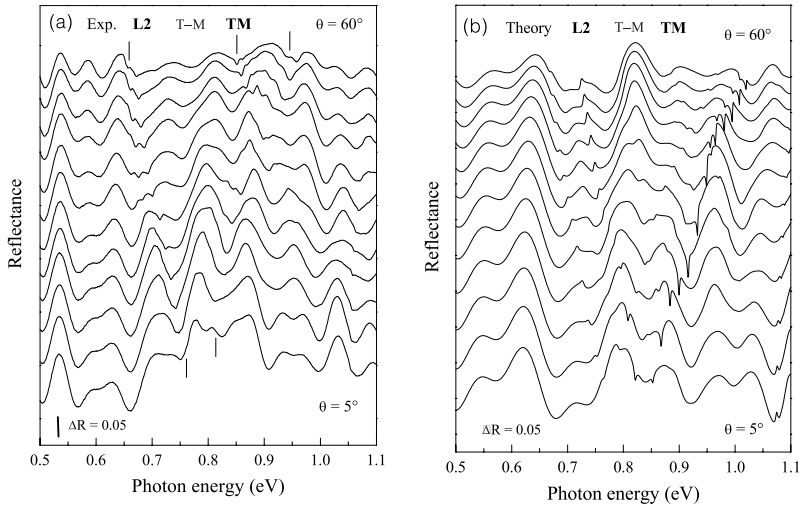

Fig. 5. Sample L2: experimental (a) and calculated (b) variable angle reflectance for TM polarized light incident along the Γ-M direction. The angle of incidence is varied in steps of 5°. The different curves are shifted vertically for clarity.

coupling strength imposes stringent matching- conditions for the excitation of quasi-guided modes.

We now come into more details about the photonic band structure of the L2 sample. As already pointed out, the dispersion of photonic bands that lie above the light line can be conveniently extracted from the energy position of the resonances *versus* the in plane wavevector **k** that spans the Brillouin zone upon varying the angle θ. Since most structures in reflectance spectra exhibit a dispersive-like shape, we took the inflection point as the energy position for the propagating mode; this leads to some uncertainty in the absolute value of the experimentally determined energy bands, which is however estimated to be in the range of a few meV. This analysis is reported in Figure 6, where the measured bands (a) are compared with photonic bands in the waveguide calculated by the methods previously described (b). Photonic bands are separated in TE and TM modes, according to mirror symmetry with respect to the plane of incidence (**k**,**z**). The frequency dispersion of the dielectric constants of GaAs and Al GaAs are taken into account in an approximate way by calculating each group of nearby bands with $\varepsilon(\omega)$ taken at an average frequency. Dotted lines represent the dispersion of photons in GaAs, AlGaAs and in air.

We emphasize that the classification of photonic modes as "TE" or "TM" follows from mirror symmetry with respect to the plane of incidence along the main symmetry directions of the Brillouin zone, and is unrelated to the conventional terminology [45] which refers instead to a horizontal mirror symmetry in a 2D photonic crystal (such symmetry is not present in an asymmetric waveguide). Since the vertical mirror plane changes when turning from the ΓX to the ΓM direction, there are some bands which appear to "stop" at the Γ point in one polarization and to restart in the other polarization.

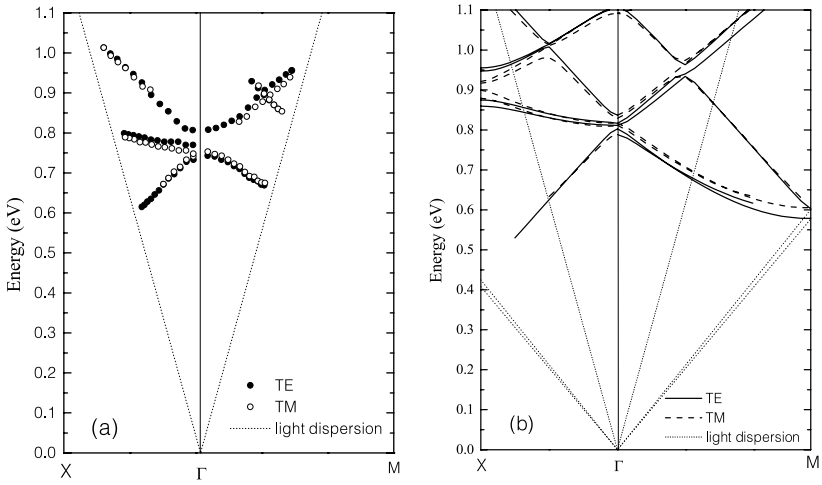

Fig. 6. Experimental (a) and calculated (b) photonic modes for sample L2, for different polarizations with respect to the plane of incidence: TE (full circles and solid lines) TM (open circles and dashed lines). Dotted lines represent the dispersion of light in air (a) and in the core and cladding (b).

Most of the calculated bands in the investigated range can be identified in the experimental spectra, and a rather good agreement for dispersion and energy values is obtained both for *even* (TM) and *odd* (TE) modes. Particularly, an anti-crossing of two bands can be clearly observed around 0.9 eV in the experimental and calculated spectra along the Γ-M direction. We notice that TE and TM bands have very similar dispersions both along the Γ-M and Γ-X directions, and exhibit rather small energy gaps at the high symmetry points of the Brillouin zone. Actually, due to the quite low air fraction of this particular sample, the system is very close to the ideal *empty lattice* or *free photon* case, where light propagation would be simply governed by an unpatterned slab waveguide with the average refractive index [25,47].

Now we turn our attention to the sample with a higher air fraction, namely RUN3. The variable angle reflectance spectra (experimental and calculated) are shown in Figures 7 and 8 for TE and TM polarized light incident along the Γ-X direction. Similar results are obtained for light incident along the Γ-M orientation (not shown here). Again, the angle of incidence θ is varied from 5° to 60° in steps of 5° and the curves are vertically shifted in order to facilitate viewing.

As can be noticed, interference fringes from the waveguide structure still characterize the reflectance spectra. The period of the interference is now much longer, due to the considerably higher air fraction and correspondingly lower refractive index. The interference pattern is again a complex superposition of core and core + cladding contributions and is well reproduced by theory with an etch depth of 0.95 μm. A large air fraction causes also that the angular dependent resonant structures are considerably broader than in sample L2. As mentioned before, broader resonances imply a larger coupling of folded modes above the light line to leaky waveguide modes, and therefore an increase of the diffraction losses outside of the waveguide. By comparing experimental with calculated spectra we found good agreement, even though in this case the calculated resonances appear to be slightly sharper than the experimental ones. This is probably due to some disorder effect introduced by the etching process.

The photonic bands of the RUN3 sample are reported in Figure 9, where experimental bands (a) are compared to the calculated ones (b). The criteria adopted for the analysis of the experimental spectra and the methods of calculation are the same as for sample L2. The overall situation, as compared to the results obtained for sample L2, is rather different. The whole band diagram is shifted to higher energies, and TE and TM bands are now well separated and show a fairly dissimilar dispersion: both features follow from the large air fraction. We notice that truly guided modes, *i.e.*, modes whose dispersion is confined between the GaAs core and the AlGaAs dispersion lines, are present both for TE and TM polarizations. However, as results from the band diagrams, the lowest bands in the guided mode region have a finite cut-off wavelength imposed by the thickness of the asymmetric waveguide. The guided modes go over smoothly into the radiative region when crossing the light line, and should thereafter be viewed as resonances or quasi-guided modes. The first order waveguide mode folded in the radiative region has gaps at the center zone and edge. Since the waveguide is asymmetric, there is no parity distinction between first and second- order modes and their energy dispersions anti-cross with very small gaps. Most of the calculated TE and TM bands up to 1.5 eV are observed in the experimental spectra, and a good agreement is achieved for the dispersion and the energy values. Small quantitative discrepancies (of the order of 0.05 eV) remain for the two high-energy anti-crossing TM bands. This, however, could be related to the fact that high-energy bands are more sensitive to the precise shape of the dielectric pattern within the unit cell. Lastly, the diagrams show a gap that opens around 1.2 eV in both polarizations over most of the Brillouin zone: the

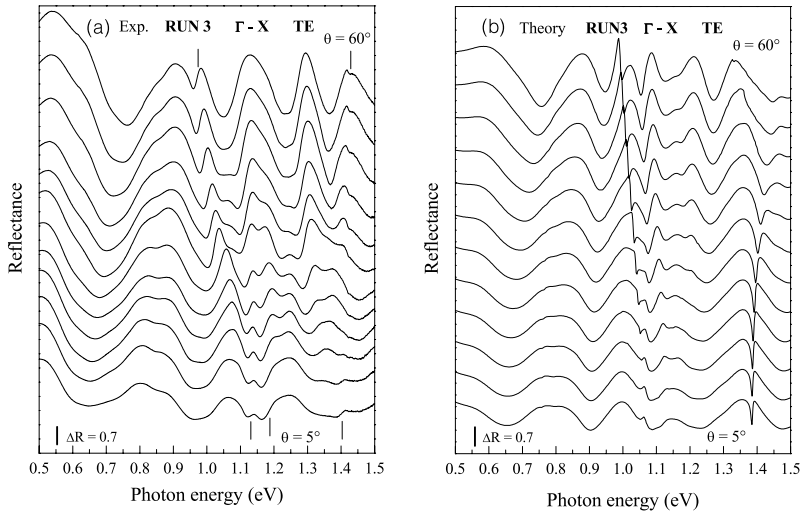

Fig. 7. Sample RUN3: experimental (a) and calculated (b) variable angle reflectance for TE polarized light incident along the Γ-X direction. The angle of incidence is varied in steps of 5°. The different curves are shifted vertically for clarity.

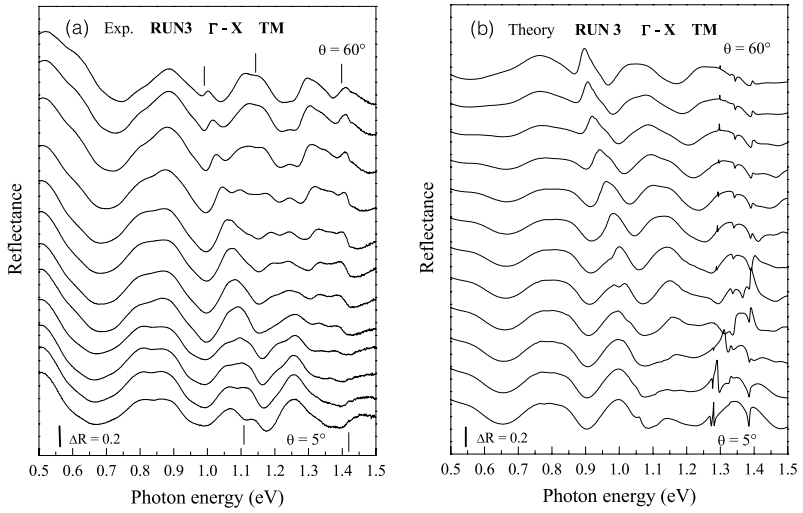

Fig. 8. Sample RUN3: experimental (a) and calculated (b) variable angle reflectance for TM polarized light incident along the Γ-X direction. The angle of incidence is varied in steps of 5°. The different curves are shifted vertically for clarity.

gap is large at the Brillouin zone center and closes only very near to the zone boundary. The photonic density of states is expected to be very low in the energy region 1.15–1.25 eV, which we may call a pseudo-gap. Linear defects in the 2D lattice would act as channel waveguides and would support propagating modes in this pseudo-gap.

5 Conclusions

Two different GaAs/AlGaAs photonic crystal waveguides have been grown and studied by optical means. The samples had 2D patterns with a square Bravais lattice but different air fractions and basis in the unit cell (defined by the refractive index variation). Spectroscopic ellipsometry on the unpatterned waveguide allowed to determine the thicknesses of the core and cladding layers. Reflectance measurements at variable angle of incidence showed resonant structures which have been attributed to the excitation of photonic modes. The dispersion of photonic bands in the patterned waveguide has been determined by following the angular evolution of the resonant structures for different orientations of the sample and polarization of light. The experimental results have been compared with theoretical calculations of the reflectance and of the photonic bands in the photonic crystal slab.

The sample L2 with a basis of air rings and an air fraction of 12% showed narrow resonant structures, indicating good guiding properties for the photonic modes above the light line. All qualitative features of the reflectance and of the photonic band dispersion are well reproduced by the theory, including anticrossings of the levels along the Γ-M orientation. The dispersion of photonic modes is similar for TE and TM polarizations and is close to that of free photons in an effective waveguide with the average dielectric constant. The sample RUN3 with a basis of tilted

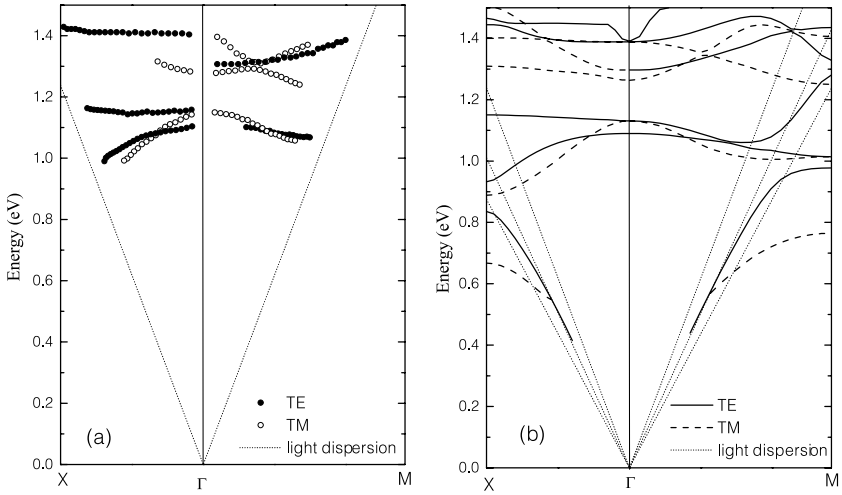

Fig. 9. Experimental (a) and calculated (b) photonic modes for sample RUN3, for different polarizations with respect to the plane of incidence: TE (full circles and solid lines) TM (open circles and dashed lines). Dotted lines represent the dispersion of light in air (a) and in the core and cladding (b).

dielectric squares and an air fraction of 72% showed broader spectral features, related to the higher radiative width and diffraction losses of quasi- guided modes above the light line. The photonic dispersion shows very good agreement with the theoretical predictions, provided that the symmetry of the photonic modes with respect to the plane of incidence is considered. The dispersion of photonic modes is strongly different for the two polarizations and shows a pseudo-gap around 1.2 eV (1 micron wavelength) where the photonic density of states is expected to be very low.

This work was supported in part by INFM PAIS 2001 project "2DPHOCRY".

References

1. T.F. Krauss, R.M. De La Rue, S. Brand, Nature **383**, 699 (1996).
2. S. Fan, P.R. Villeneuve, J.D. Joannopoulos, E.F. Schubert, Phys. Rev. Lett. **78**, 3294 (1997).
3. D. Labilloy, H. Benisty, C. Weisbuch, T.F. Krauss, R.M. De La Rue, V. Bardinal, R. Houdré, U. Oesterle, D. Cassagne, C. Jouanin, Phys. Rev. Lett. **79**, 4147 (1997).
4. D. Labilloy, H. Benisty, C. Weisbuch, C.J.M. Smith, T.F. Krauss, R. Houdré, U. Oesterle, Phys. Rev. B **59**, 1649 (1999).
5. H. Benisty, C. Weisbuch, D. Labilloy, M. Rattier, C.J.M. Smith, T.F. Krauss, R.M. De La Rue, R. Houdré, U. Oesterle, C. Jouanin, D. Cassagne, J. Lightwave Technol. **17**, 2063 (1999).
6. S.G. Johnson, S. Fan, P.R. Villeneuve, J.D. Joannopoulos, L.A. Kolodziejski, Phys. Rev. B **60**, 5751 (1999).
7. T. Baba, N. Fukaya, J. Yonekura, Electron. Lett. **27**, 654 (1999).
8. V.N. Astratov, D.M. Whittaker, I.S. Culshaw, R.M. Stevenson, M.S. Skolnick, T.F. Krauss, R.M. De La Rue, Phys. Rev. B **60**, R16225 (1999).
9. V.N. Astratov, I.S. Culshaw, R.M. Stevenson, D.M. Whittaker, M.S. Skolnick, T.F. Krauss, R.M. De La Rue, J. Lightwave Technol. **17**, 2050, (1999).
10. D.M. Whittaker, I.S. Culshaw, Phys. Rev. B **60**, 2610 (1999).
11. V.N. Astratov, R.M. Stevenson, I.S. Culshaw, D.M. Whittaker, M.S. Skolnick, T.F. Krauss, R.M. De La Rue, Appl. Phys. Lett. **77**, 178 (2000).
12. H. Benisty, D. Labilloy, C. Weisbuch, C.J.M. Smith, T.F. Krauss, D. Cassagne, A. Béraud, C. Jouanin, Appl. Phys. Lett. **76**, 532 (2000).
13. M. Tokushima, H. Kosaka, A. Tomita, H. Yamada, Appl. Phys. Lett. **76**, 952 (2000).
14. M. Lončar, D. Nedeljković, T. Doll, J. Vučković, A. Scherer, T.P. Pearsall, Appl. Phys. Lett. **77**, 1937 (2000).
15. V. Pacradouni, W.J. Mandeville, A.R. Cowan, P. Paddon, J.F. Young, S.R. Johnson, Phys. Rev. B **62**, 4204 (2000).
16. T. Søndergaard, A. Bjarklev, M. Kristensen, J. Erland, J. Broeng, Appl. Phys. Lett. **77**, 785 (2000).
17. E. Chow, S.Y. Lin, S.G. Johnson, P.R. Villeneuve, J.D. Joannopoulos, J.R. Wendt, G.A. Vawter, W. Zubrzycki, H. Hou, A. Alleman, Nature **407**, 983 (2000).
18. E. Silvestre, J.M. Pottage, P.St. J. Russell, P.J. Roberts, Appl. Phys. Lett. **77**, 942 (2000).
19. D.J. Ripin, Kuo-Yi Lim, G.S. Petrich, P.R. Villeneuve, S. Fan, E.R. Thoen, J.D. Joannopoulos, E.P. Ippen, L.A. Kolodziejski, J. Appl. Phys. **87**, 1578 (2000).
20. Han-Youl Ryu, Jeong-Ki Hwang, Yong-Hee Lee, J. Appl. Phys. **88**, 4941 (2000).
21. D. Coquillat, A. Ribayrol, R.M. De La Rue, M. Le Vassor d'Yerville, D. Cassagne, C. Jouanin, Phys. Status Solidi (a) **183**, 135 (2001).
22. N. Kawai, K. Inoue, N. Ikeda, N. Carlsson, Y. Sugimoto, K. Asakawa, S. Yamada, Y. Katayama, Phys. Rev. B **63**, 153313 (2001).
23. N. Kawai, K. Inoue, N. Carlsson, N. Ikeda, Y. Sugimoto, K. Asakawa, T. Takemori, Phys. Rev. Lett. **86**, 2289 (2001).

24. T. Ochiai, K. Sakoda, Phys. Rev. B **63**, 125107 (2001).
25. T. Ochiai, K. Sakoda, Phys. Rev. B **64**, 45108 (2001).
26. S. Olivier, M. Rattier, H. Benisty, C. Weisbuch, C. J. M. Smith, R. M. De La Rue, T. F. Krauss, U. Oesterle, R. Houdré, Phys. Rev. B **63**, 113311 (2001).
27. M. Agio, C.M. Soukoulis, Phys. Rev. E **64**, 55603 (2001).
28. M. Qiu, K. Azizi, A. Karlsson, M. Swillo, B. Jaskorzynska, Phys. Rev. B **64**, 165105 (2001).
29. S. Yamada, T. Koyama, Y. Katayama, N. Ikeda, Y. Sugimoto, K. Asakawa, N. Kawai, K. Inoue, J. Appl. Phys. **89**, 855 (2001).
30. Ph. Lalanne, H. Benisty, J. Appl. Phys. **89**, 1512 (2001).
31. S. Lan, S. Nishikawa, H. Ishikawa, O. Wada, J. Appl. Phys. **90**, 4321 (2001).
32. S. Olivier, H. Benisty, M. Rattier, C. Weisbuch, M. Qiu, A. Karlsson, C.J.M. Smith, R. Houdré , U. Oesterle, Appl. Phys. Lett. **79**, 2514 (2001).
33. P.R. Villeneuve, M. Piché, Phys. Rev. B **46**, 4969 (1992); *ibid.* **46**, 4973 (1992).
34. R. Padjen, J.-M. Gérard, J.-Y. Marzin, J. Mod. Opt. **41**, 295 (1994).
35. C.M. Anderson, K.P. Giapis, Phys. Rev. Lett. **77**, 2949 (1996); Phys. Rev. B **56**, 7313 (1997).
36. X.-H. Wang, B.-Y. Gu, Z.-Y. Li, G.-Z. Yang, Phys. Rev. B **60**, 11417 (1999).
37. M. Agio, L.C. Andreani, Phys. Rev. B **61**, 15519 (2000).
38. R. Wang, X.-H. Wang, B.Y. Gu, G.-Z. Yang, J. Appl. Phys. **90**, 4307 (2001).
39. L.C. Andreani, M. Agio, IEEE J. Quantum Electron., 2002, in press.
40. F. Romanato, L. Businaro, E. Di Fabrizio, A. Passaseo, M. De Vittorio, R. Cingolani, M. Patrini, M. Galli, D. Bajoni, L.C. Andreani, submitted.
41. K.M. Ho, C.T. Chan, C.M. Soukoulis, Phys. Rev. Lett. **65**, 3152 (1990).
42. *Handbook of optical constants of solids*, edited by E.D. Palik (Academic Press, Orlando, 1985).
43. W.M. Robertson, G. Arjavalingam, R.D. Meade, K.D. Brommer, A.M. Rappe, J.D. Joannopoulos, J. Opt. Soc. Am. B **10**, 322 (1994).
44. K. Sakoda, Phys. Rev. B **52**, 7982 (1995).
45. J.D. Joannopoulos, R.D. Meade, J.N. Winn, *Photonic Crystals–Molding the Flow of Light* (Princeton University Press, 1995).
46. M. Patrini, M. Galli, F. Marabelli, M. Agio, L.C. Andreani, D. Peyrade, Y.Chen, IEEE J. Quantum Electron., 2002, in press.
47. L. Liu, J.T. Liu, Eur. Phys. J. B **9**, 381 (1999).